tvst

Article

Recognizing Atrophy and Mixed-Type Neovascularization in Age-Related Macular Degeneration Via Clinicopathologic Correlation

Ling Chen[1,2], Miaoling Li[2], Jeffrey D. Messinger[1], Daniela Ferrara[3], Christine A. Curcio[1], and K. Bailey Freund[4–7]

[1] Department of Ophthalmology and Visual Sciences, University of Alabama at Birmingham School of Medicine, Birmingham, Alabama, USA
[2] State Key Laboratory of Ophthalmology, Zhongshan Ophthalmic Center, Sun Yat-sen University, Guangzhou, China
[3] Genentech, South San Francisco, California, USA
[4] Vitreous Retina Macula Consultants of New York, New York, New York, USA
[5] LuEsther T. Mertz Retinal Research Center, Manhattan Eye, Ear and Throat Hospital, New York, New York, USA
[6] Department of Ophthalmology, New York University School of Medicine, New York, New York, USA
[7] Columbia University College of Physicians and Surgeons, Harkness Eye Institute, New York, New York, USA

Correspondence: Christine A. Curcio, Department of Ophthalmology and Visual Sciences, EyeSight Foundation of Alabama Vision Research Laboratories, 1670 University Boulevard Room 360, University of Alabama School of Medicine, Birmingham, AL 35294-0099, USA. e-mail: christinecurcio@uabmc.edu

Received: February 26, 2020
Accepted: May 20, 2020
Published: July 7, 2020

Keywords: age-related macular degeneration; neovascularization; photoreceptors; retinal pigment epithelium; Müller glia; choriocapillaris; gliosis; atrophy; transdifferentiation; optical coherence tomography; fluorescein angiography

Citation: Chen L, Li M, Messinger JD, Ferrara D, Curcio CA, Freund KB. Recognizing atrophy and mixed-type neovascularization in age-related macular degeneration via clinicopathologic correlation. Trans Vis Sci Tech. 2020;9(8):8, https://doi.org/10.1167/tvst.9.8.8

Purpose: We explored via multimodal imaging and histology an eye with mixed-types 1 and 2 macular neovascularization (MNV) and complete retinal pigment epithelium (RPE) and outer retinal atrophy (cRORA) in age-related macular degeneration.

Methods: An 82-year-old white man was followed 7 years by optical coherence tomography and treated with intravitreal anti-vascular endothelial growth factor for 3 years. At the last clinic visit, visual acuity was stable at 20/50. Two months later the patient died, and eyes were preserved at 8.33 hours after death. Submicrometer epoxy resin sections of osmicated tissue were stained with toluidine blue and evaluated by oil immersion microscopy.

Results: A shallow irregular RPE elevation on optical coherence tomography correlated with type 1 MNV with fibrocellular scar and neocapillaries (close to RPE), at a density similar to underlying native choriocapillaris (0.37 vs. 0.42). Type 2 MNV covered the native RPE and was enveloped at the margins by RPE, without neocapillaries. Native RPE cells transdifferentiated from age-normal to melanotic and entered type 1 MNV and choroid. Some photoreceptors persisted over MNV. The cRORA initiated at a collapsed druse, expanded during follow-up, and exhibited low choriocapillaris density (0.05).

Conclusions: An eye with maintained vision on 3 years of anti-vascular endothelial growth factor therapy had type 1 MNV sustaining RPE. Type 2 MNV enveloped by RPE was visible in optical coherence tomography and histology. Persistence of photoreceptors and RPE over MNV contrasted with drusen-associated cRORA.

Translational Relevance: Vision during long-term anti-vascular endothelial growth factor treatment persists by MNV partially preserving outer retinal cells and by RPE enveloping type 2 MNV.

Introduction

Age-related macular degeneration (AMD) is a leading cause of visual loss in older persons worldwide.[1] Macular neovascularization (MNV) is a major sight-threatening complication of AMD that is also treatable.[2] Intravitreal injections of anti-vascular endothelial growth factor (VEGF) agents are the current standard of care for treating neovascular AMD.[2] Although visual outcomes with intravitreal anti-VEGF therapy are far superior to those achieved with prior treatments, some eyes ultimately lose central vision owing to macular atrophy, that is, atrophy of the RPE and overlying photoreceptors.[3]

According to the Consensus on Neovascular Age-Related Macular Degeneration Nomenclature Study Group,[4] type 1 MNV originates from the choroid and proliferates beneath the retinal pigment epithelium (RPE) and its basal lamina (BL, henceforth "RPE-BL")[5,6] and above the inner collagenous layer of Bruch's membrane (BrM).[7,8] In this space, type 1 MNV closely apposes RPE and has ultrastructural specializations for exchange (neochoriocapillaris[9]). When type 1 MNV extends across the RPE-BL into the subretinal space, it is termed type 2 MNV. Type 3 MNV originates from retinal vessels in the deep vascular complex and infiltrates the sub–RPE-BL space.[10] Type 1 and type 2 MNV correspond with poorly defined (occult) and well-defined (classic) neovascular lesions, respectively, on fluorescein angiography. The advent of spectral domain optical coherence tomography (OCT) has facilitated visualization of retinal structure and MNV lesions. Types 1, 2, and 3 are now the OCT-based categorization of MNV. If prominent MNV is present in the subretinal and sub-RPE compartments, the term mixed type 1 and type 2 MNV can be applied.[4]

Our cellular level understanding of macular atrophy could be furthered by comparison with and differentiation from other forms of RPE atrophy. The term complete RPE and outer retinal atrophy (cRORA) (RPE atrophy >250 µm) was proposed as a descriptor for atrophy regardless of cause by the international Classification of Atrophy Meetings group.[4,11] The clinical course of drusen-associated atrophy is now well-documented through high-resolution histology coupled with longitudinal clinical imaging. These studies suggest that soft drusen have multiple fates, including replacement with avascular fibrosis, formation of cholesterol crystals and calcific nodules in the sub–RPE-BL space, and invasion by Müller glia after death of RPE to clear remaining druse material.[12–15] Earlier in the atrophic process, RPE cells exhibit stereotypic morphologies in distinct pathways of cell fate, including anterior migration, basolateral shedding of granule aggregates, and loss of autofluorescent granules.[16–18] In contrast with atrophy in non-neovascular AMD, macular atrophy in neovascular AMD exhibits transdifferentiation of RPE to distinct morphologies not found in atrophic AMD and an oblique rather than curved descent of the external limiting membrane (ELM) toward the BrM.[19–21]

Herein we report multimodal clinical imaging and high-resolution histology of an eye with both drusen-associated atrophy and mixed type 1 and type 2 MNV. Long-term OCT follow-up of this eye revealed the chronology and characteristics of drusen collapse, atrophy expansion, MNV initiation, and treatment with intravitreal anti-VEGF therapy. To correlate OCT and histology, we evaluated features seen on OCT B-scans and histology sections. High-resolution histology sections were used to study characteristics of type 1 and 2 MNV, drusen-associated atrophy and a transitional region around it, and neural retina and RPE-choriocapillaris (ChC) changes. Our data suggest that long-term anti-VEGF treatment may support vision via partial preservation of the outer retinal cells and RPE envelopment of type 2 MNV. RPE transdifferentiation and choroidal invasion by RPE and Müller glia are new aspects of atrophy seen in this case.

Methods

Compliance

A retrospective review of medical records and imaging data and the histopathology study were approved by the institutional review boards of the Manhattan Eye, Ear, and Throat Hospital/Northwell Health and the University of Alabama at Birmingham. All study components complied with the Health Insurance Portability and Accountability Act of 1996 and adhered to the tenets of the Declaration of Helsinki. Written informed consent was obtained from the patient.

Clinical Course

Figures 1 and 2 document multimodal clinical imaging of the index eye, the right eye of a man of European descent. At age 69 the patient presented with bilateral non-neovascular AMD, and a lamellar macular hole (LMH) along with lamellar hole–associated epiretinal proliferation (LHEP)[22] in the left eye. Medical history included hypertension and hypothyroidism. At age 72, a LMH with LHEP was diagnosed in the right eye. The histopathologic

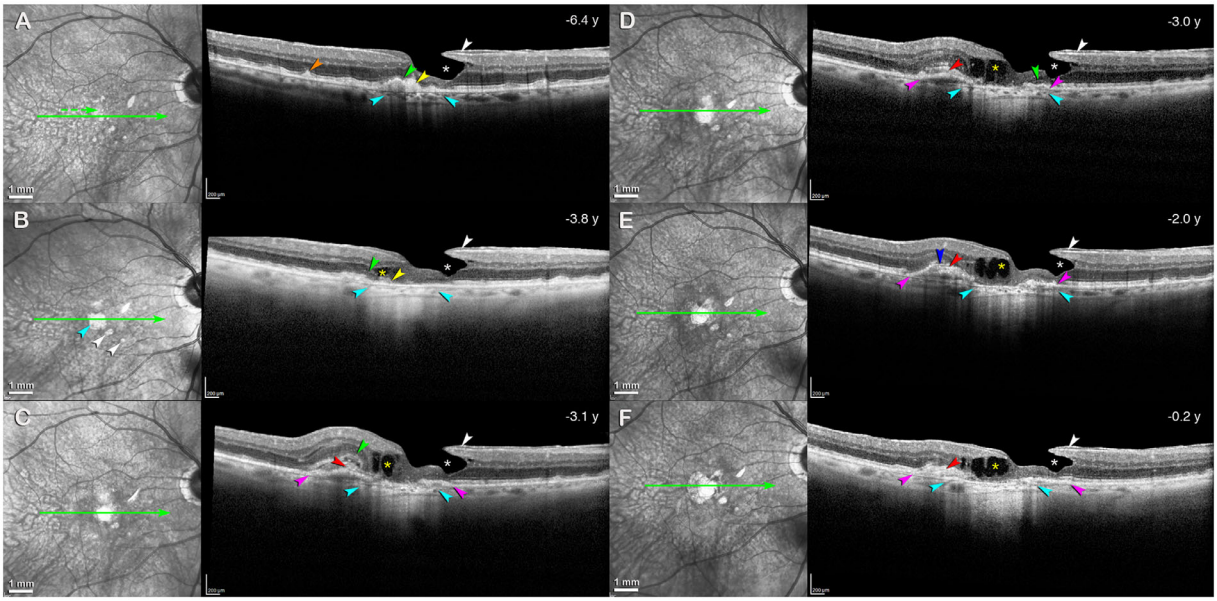

Figure 1. Expansion of atrophy and incident neovascularization. Near-infrared reflectance (NIR, first and third columns) with corresponding OCT B-scans (second and fourth columns) through a foveal location (indicated by green arrows) tracked over 6.2 years. The dashed green arrow in A indicates the location of B-scans shown in each individual panel in Figure 4. All B-scans were obtained at the same fundus location to show chronology of lesion development. Time in years before patient death is indicated. Lamellar hole (white asterisks) and lamellar hole-associated epiretinal proliferation on the surface of internal limiting membrane was stable over time. Choroidal hypertransmission (teal arrowheads), started as pinstripes in A, became nearly uniform in B corresponding with a reflective large area of atrophy on NIR (teal arrowhead in B), and expanded over time. White arrowheads in B show two smaller atrophic spots. (A) Subretinal drusenoid deposits (orange arrowhead) in the temporal macula and soft drusen (yellow arrowhead) in the central macula with an ELM descent on top (green arrowhead). Best-corrected visual acuity (BCVA): 20/30. (B) Soft drusen collapsed with a legacy of atrophy (yellow arrowhead), a visible ELM descent (green arrowhead), and intraretinal cysts. BCVA: 20/40. (C–F) Pink arrowhead, SIRE (originally called double-layer sign) corresponding to type 1 MNV; red arrowhead, subretinal hyperreflective material (SHRM) corresponding to type 2 MNV; yellow asterisk, intraretinal fluid. (C) A SIRE and SHRM were detected with increased intraretinal fluid, considered the onset of exudative activity, which was then treated with intravitreal ranibizumab. An ELM descent was faintly visible (green arrowhead). BCVA: 20/50. (D) One month after treatment, SHRM was retracted with persistent intraretinal fluid. An ELM descent was visible on the other side (green arrowhead). BCVA: 20/70. (E) A hyperreflective band (blue arrowhead) was indicated at the temporal side of SHRM. No ELM descent was visible. BCVA: 20/40. (F) At the last clinical visit, SHRM on top of SIRE can still be observed, without a visible ELM descent. BCVA: 20/50.

findings associated with LMH and LHEP will be reported in a separate study. At age 81, he underwent cataract surgery in both eyes. Tracked spectral domain OCT (30° × 20° OCT volume, 19 scans, 240 µm spacing, automated real-time averaging 12-30; Heidelberg Spectralis HRA+OCT, Heidelberg Engineering, Heidelberg, Germany) of the right eye was obtained at each visit after the patient turned 82. OCT at this time showed soft drusen and thin stripes of hypertransmission into the choroid (Fig. 1A), signifying highly focal RPE degeneration.[23] Two and one-half years later, the druse had collapsed with a legacy of cRORA, evidenced by uniform hypertransmission, as well as intraretinal cysts (Fig. 1B).

At age 86, he developed symptomatic neovascular AMD. At the time of conversion, best-corrected visual acuity in this eye was 20/50, a decrease of 1 line compared with the examination 6 months prior. Color fundus photography showed scattered drusen with central hypopigmentation (Fig. 2A). Fluorescein angiography (Topcon TRC-50IX fundus camera; Topcon, Tokyo, Japan) showed both well-defined (classic) and poorly defined (occult) neovascular lesion components (Figs. 2B–2D). Tracked OCT demonstrated a persistent LMH and LHEP with new findings of a shallow irregular RPE elevation (SIRE), subretinal hyperreflective material, new subretinal fluid, and retinal edema (Fig. 1C). From then forward, the right eye of this 86-year-old patient was managed with continuous intravitreal ranibizumab (0.5 mg /0.05 mL) on a treat-and-extend regimen, receiving 28 injections over 36 months (Figs. 1D-F). The patient was last examined and injected at 89 years of age, 19.3 years after presentation and 2 months before death. At this visit, tracked OCT of the right eye showed a stable LMH and LHEP,

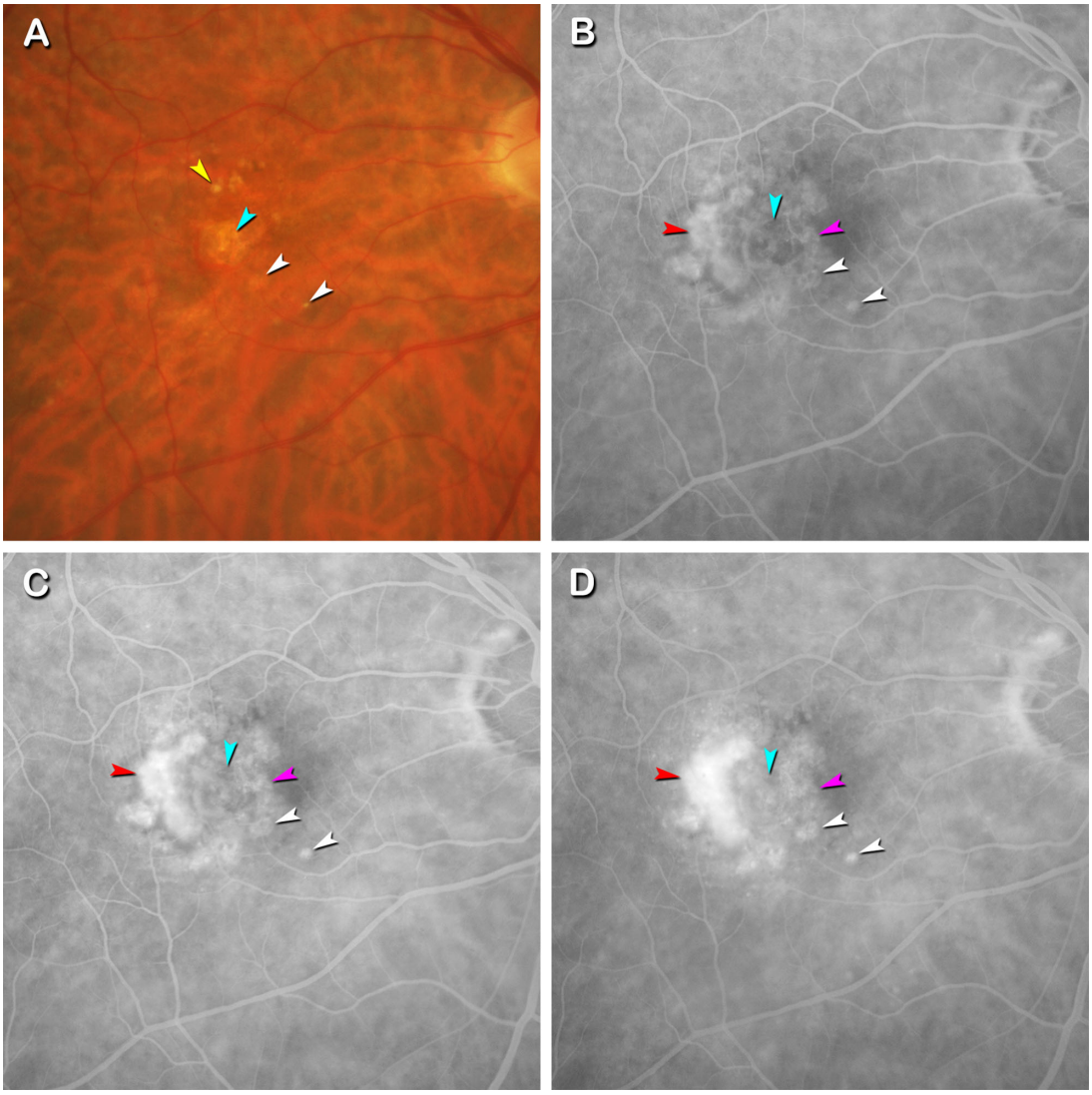

Figure 2. Pretreatment fluorescein angiography showing classic and occult MNV and atrophy. Images were acquired 3.1 years before patient death. (A) Color fundus photograph shows drusen in superior macula (yellow arrowhead), an oval atrophic area in the central macula (teal arrowhead), and two nearby small atrophic spots (white arrowheads). (B–D) Fluorescein angiography in early, mid and late phases show both well-defined (classic, red arrowheads) and poorly defined (occult, pink arrowheads) neovascular lesion components. These encompass a centrally located atrophic area (teal arrowhead). Two nearby small atrophic spots were hyperfluorescence owing to window defects (white arrowheads).

persistent SIRE with overlying subretinal hyperreflective material, and small cysts in the Henle fiber layer (HFL). In addition, choroidal hypertransmission (atrophy) expanded over time (Fig. 1F). Noted on Figs. 1 and 2, without comment in the record, are three atrophic spots, the largest meeting criteria for cRORA. Final best-corrected visual acuity of this eye was 20/50.

The Supplementary Figure shows clinical imaging in the left eye demonstrating a similar course and greater preservation of outer retinal structure, yet poorer acuities, attributed to inner retinal pathology.

Tissue Preparation

Two months after the last clinical examination, the patient died of cardiopulmonary arrest secondary to Alzheimer's disease. Globes were recovered 8.33 hours after death by personnel of The Eye-Bank for Sight Restoration (New York, NY), opened anteriorly by cornea removal, preserved by immersion in 4% phosphate buffered paraformaldehyde, and shipped overnight on wet ice to Birmingham, Alabama.

The preserved globe with anterior segment removed was imaged with ex vivo OCT and NIR (787 nm)

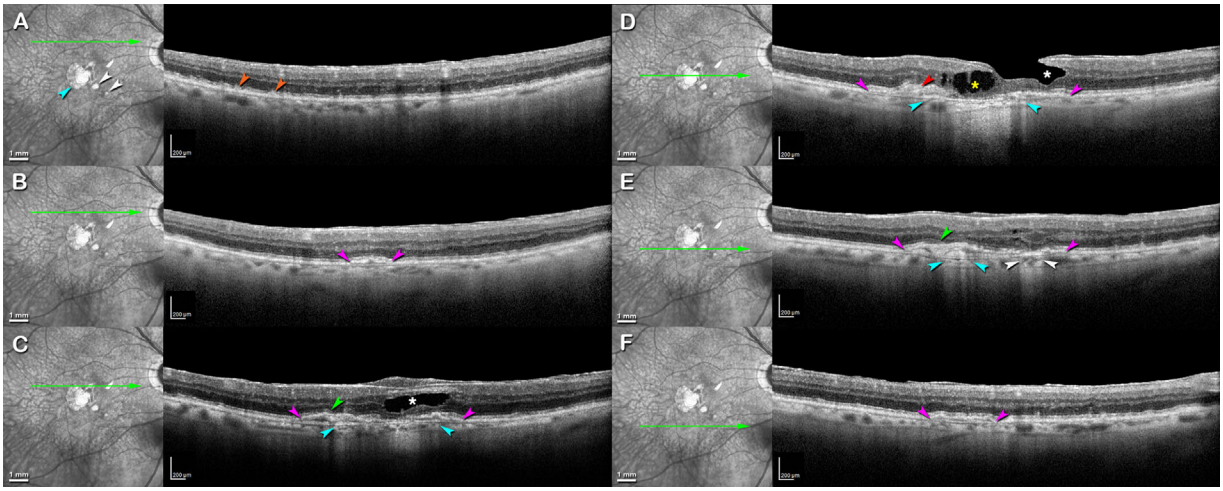

Figure 3. Last clinic visit of an eye with atrophy, neovascular AMD, and lamellar hole-associated epiretinal proliferation. Images were acquired 2 months before patient death. Near-infrared reflectance (NIR, first and third columns) with green arrows indicating the locations of corresponding OCT B-scans (second and fourth columns). (A) NIR shows three atrophic spots: large (teal arrowhead), and two small (white arrowheads). In the B-scan, orange arrowheads indicate subretinal drusenoid deposits in the superior macula. (B–F) B-scans show a SIRE (originally called double-layer sign, pink arrowheads). (C–E) B-scans through the central macula show lamellar hole (white asterisks), intraretinal cysts (yellow asterisk) and development of homogeneous choroidal hypertransmission under the large atrophic spot (teal arrowheads). Green arrowheads in C and E indicating ELM descents that are visible in some sections. Red arrowhead in D indicates subretinal hyperreflective material on top of RPE. White arrowheads in E reveal choroidal hypertransmission owing to the medium atrophic spot.

before histologic processing, as described.[7] An 8-mm diameter full-thickness tissue sample including the fovea and most of the optic nerve head was excised from the eyecup, post-fixed with osmium tannic acid paraphenylenediamine to preserve extracellular lipids,[24] embedded in epoxy resin (PolyBed 812, EMS, Hatfield, PA), and oriented for sectioning in a superior to inferior direction. Glass slides ($n = 33$) with 0.8-µm-thick sections (distance, 131 ± 44 µm; range, 60–240 µm) were stained with toluidine blue. One section per slide was scanned with a 20× objective and a robotic microscope stage (Olympus VSI 120, CellSens; Olympus, Center Valley, PA), scaled to tissue units, and centered on the fovea or vertical meridian (where the Henle fibers diverge) using a custom plugin for ImageJ (https://imagej.nih.gov/ij/download.html). Sections were then scanned using a 60× oil-immersion objective (numerical aperture = 1.42) and viewed on a monitor at magnifications up to 1240× using ImageJ. For figures, images were adjusted to maximize the intensity histogram for contrast and white balance (Photoshop CS6, Adobe Systems, San Jose, CA).

Histopathologic Review

Ex vivo OCT B-scans (described elsewhere in this article) were referenced to the in vivo OCT B-scans from the last clinic visit (2 months before death). The in vivo OCT B-scans were used as a reference for histology sections, with constraints owing to almost complete postmortem retinal detachment. Neural retina and RPE-choroid appearing on the same glass slide were not necessarily correlated with the same OCT B-scan owing to lateral torsion around a point of attachment at the optic nerve head. Because point-by-point OCT–histology correlation[25] was not possible, we compared the extent and serial order of features on 19 in vivo OCT B-scans (labeled 1–19) to the extent and serial order of features on 19 evenly spaced histology sections (labeled a–s) through roughly the same area. ChC density (proportion of BrM or RPE covered) in native ChC underneath MNV, ChC inside type 1 MNV, and native ChC underneath atrophy were assessed using a custom image J plugin.[9]

Results

Representative OCT B-scans at the last clinical visit are shown in Figure 3, and the distribution of clinical features on 19 B-scans are shown in Table 1. SIRE can be observed on 13 of 19 B-scans (Figs. 3B–3F), with choroidal hypertransmission and ELM descent within the SIRE area (Figs. 3C–3E). Subretinal drusenoid deposits are seen on all B-scans as granular reflective material between the RPE and the ellipsoid zone

Table 1. Distribution of Features on 19 Horizontal OCT B-Scans Obtained at the Last Clinical Visit

	Scan No.																		
OCT Feature	1	2	3	4	5	6	7	8	9	10	11	12	13	14	15	16	17	18	19
LHEP	x	x	x	x	x	x	x	x	x	x	x	x	x	x	x	x	x	x	x
Lamellar hole						x	x	x	x	x	x	x							
Intraretinal hyperreflective specks/foci	x	x	x	x	x	x	x	x	x	x	x	x	x	x	x	x	x	x	x
ELM descent					x	x	x	x	x	x	x		x						
Monés hyporeflective wedge							x	x											
SDD	x	x	x	x	x	x	x	x	x	x	x	x	x	x	x	x	x	x	x
SHRM							x	x			x								
Plateau													x						
SIRE			x	x	x	x	x	x	x	x	x	x	x	x	x				
Hypertransmission				x	x	x	x	x	x	x	x	x	x						
Hyporeflective band at the choroidal-scleral junction	x	x	x	x	x	x	x	x	x	x	x	x	x	x		x			x

LHEP, lamellar hole-associated epiretinal proliferation; SDD, subretinal drusenoid deposit; SHRM, subretinal hyperreflective material.

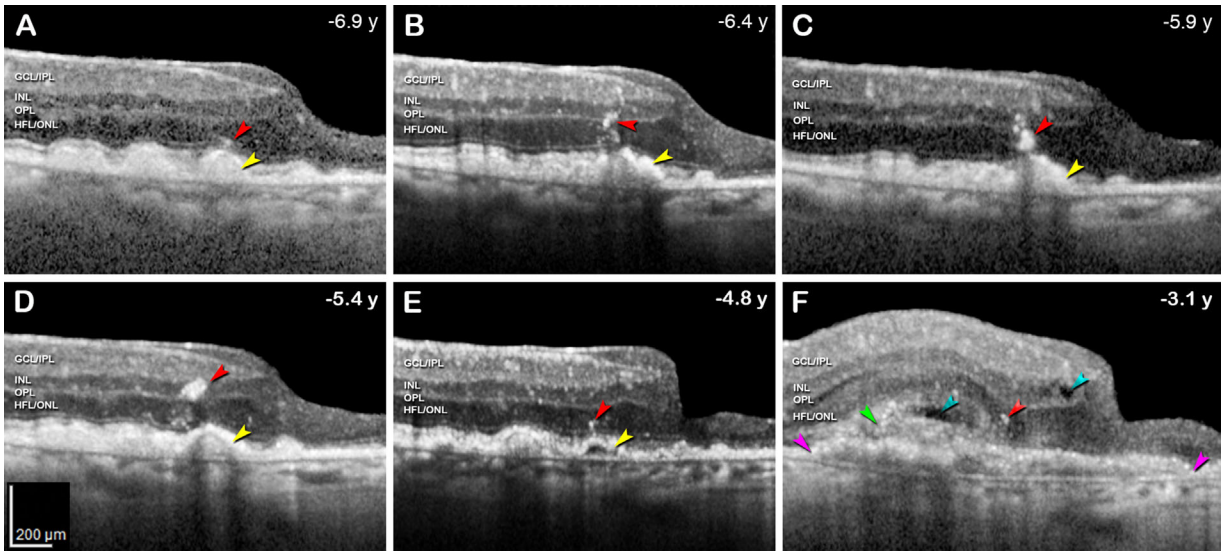

Figure 4. Chronology and characteristics of drusen collapse and incident neovascularization. OCT B-scans through a foveal location (indicated by a dashed green arrow in Fig. 1A), tracked over 3.8 years. Time in years before patient death is indicated. Red arrowhead, HRF; yellow arrowhead, soft drusen. Retinal layers: GCL/ IPL, ganglion cell and inner plexiform layer, not separable in all scans; INL, inner nuclear layer; OPL, outer plexiform layer, HFL/ONL, Henle fiber and ONL, not separable in all scans. (A) Several soft drusen in the temporal macula, with HRF (representing RPE migration) above the ELM atop one druse. (B) Soft drusen become confluent, with HRF crossing the HFL and penetrating the INL. The RPE band increases in reflectivity (C) Large HRF back-shadow and obscure the RPE band atop these confluent soft drusen. (D) Confluent soft drusen with large HRF in the INL and group of small hyperreflective specks in the ONL/HFL. (E) Soft drusen collapsed, leaving a hyporeflective interior. Small HRF remain in the ONL. (F) In a nearby scan at the same timepoint as Figure 1C, a SIRE (pink arrowheads) and subretinal hyperreflective material (SHRM, green arrowhead) developed with intraretinal and subretinal fluid (teal arrowheads). Hyperreflective foci can still be observed above SIRE. ELM on top of drusen is visible in A–E and then is not visible in F.

(stage 1) and reflective deposits that elevate (stage 2) or penetrate (stage 3) the ellipsoid zone. Also seen on the inner retinal surface of all B-scans are LHEP, with a LMH on B-scans through the central macula (Figs. 3C–3E). Of three atrophic spots in the macular region (Fig. 3), the largest, meeting cRORA criteria, was partly overlapped by the inferotemporal part of the LMH. Tracked OCT B-scans during 6.9 years follow-up disclosed that all three atrophic spots began at drusen. Fig. 4 shows hyperreflective foci (HRF) emerging from one soft druse for 2.1 years preceding druse collapse, which was followed 1.7 years later by type 1 MNV and exudation in the same topography. The cRORA centered on this druse was 0.35 mm^2

Table 2. Distribution of Features in Neural Retina on 19 Histology Sections

Section No.	a	b	c	d	e	f	g	h	i	j	k	l	m	n	o	p	q	r	s
LHEP	x	x	x	x	x	x	x	x	x	x	x	x	x	X	x	x	x	x	x
Cavitation							x	x	x	x	x	x	x						
Atrophy/ELM descent						x	x	x	x	x	x	x	x	X					
ONL thinning outside ELM descent						x	x	x	x	x	x	x	x	X					
RPE cells/granules												x							

LHEP, lamellar hole-associated epiretinal proliferation. Atrophy, absence of continuous RPE layer ≥250 µm.

Table 3. The Distribution of Features in RPE and Choroid on 19 Histology Sections

Section No.	a	b	c	d	e	f	g	h	i	j	k	l	m	n	o	p	q	r	s
Type 2 MNV			x	x	x	x	x	x											
Type 1 MNV	x	x	x	x	x	x	x	x	x	x	x	x	x	x					
RPE atrophy ≥250 µm				x	x	x	x	x	x										
Plateau						x													
SDD	x	x	x	x	x	x	x	x	x	x	x	x	x	x	x	x	x	x	x
Definite BLinD	x	x	x	x	x	x	x		x		x	x	x	x			x	x	x
Definite soft drusen	x	x		x	x	x			x		x	x	x				x	x	x
BrM thinning			x	x	x		x	x	x	x		x	x	x					
BrM defect			x	x	x	x	x	x	x	x									
Presumed Müller glia above RPE-BL				x	x	x	x												
Presumed Müller glia under RPE-BL			x		x	x	x												
Presumed Müller glia in choroid					x	x													
Lipid globule in choroid								x			x				x				x
Lipid globule in sclera	x		x	x	x		x	x	x	x	x		x						x

SDD, subretinal drusenoid deposit; BLinD, basal linear deposit.

RPE atrophy ≥250 µm, absence of continuous RPE layer ≥250 µm.

In some areas, the sub–RPE-BL space retained the shape of pre-mortem drusen and BLinD but the contents were lost in processing. Only areas with contents are shown here.

at the time of MNV conversion and 1.74 mm^2 at the last clinical visit, as measured in the OCT instrument software, for a growth rate of 0.46 mm^2/y (effective radius growth rate:[26] 0.137 mm/y). Other OCT features observed at the last visit are a hyporeflective band at the choroidal-scleral junction (16/19 B-scans) and on fewer (1–3) B-scans, a Monés hyporeflective wedge,[27] subretinal hyperreflective material, and plateau.[28]

In 19 histology sections of neural retina (Table 2), LHEP appears on all sections, with cavitation (corresponding with LMH), ELM descent and outer nuclear layer (ONL) thinning in the outer junctional zone appearing in the middle 7 to 9 sections. RPE cells/granules in the retina were observed once (Table 2). In 19 histology sections of RPE–choroid (Table 3), type 1 MNV extends over the inferior 14 sections, encompassing a smaller area of type 2 MNV and RPE atrophy 250 µm or more (six overlapping sections in the middle). Subretinal drusenoid deposits, basal linear deposit, and soft drusen were abundant across the sampled area. We also noted BrM thinning, BrM defects, and lipid globules[29] in the choroid and sclera (Table 3). A sub–RPE-BL invasion of presumed Müller glia is presented.

Figure 5 shows a mixed type 1 and 2 MNV on a section passing through the inferior macula. Type 1 MNV with fibrocellular scar and neochoriocapillaries subjacent to the RPE-BL was correlated with SIRE on OCT (Fig. 5B). Native RPE and BLamD covered the type 1 MNV. Type 2 MNV in turn covered the top of the RPE and was enveloped at the margins by RPE lacking BLamD that reflected back along the surface of the fibrovascular tissue (Fig. 5B). A BLamD defect was visible at the right (nasal) side of the fibrovascular tissue (Fig. 5B). Several vessel lumens and many pericytes were found inside type 2 MNV tissue (Fig. 5C). Type 2 MNV differs from type 1 MNV, which features neochoriocapillaris (Figs. 5B, 5C), by lacking neovessels aligned along the enveloping RPE.

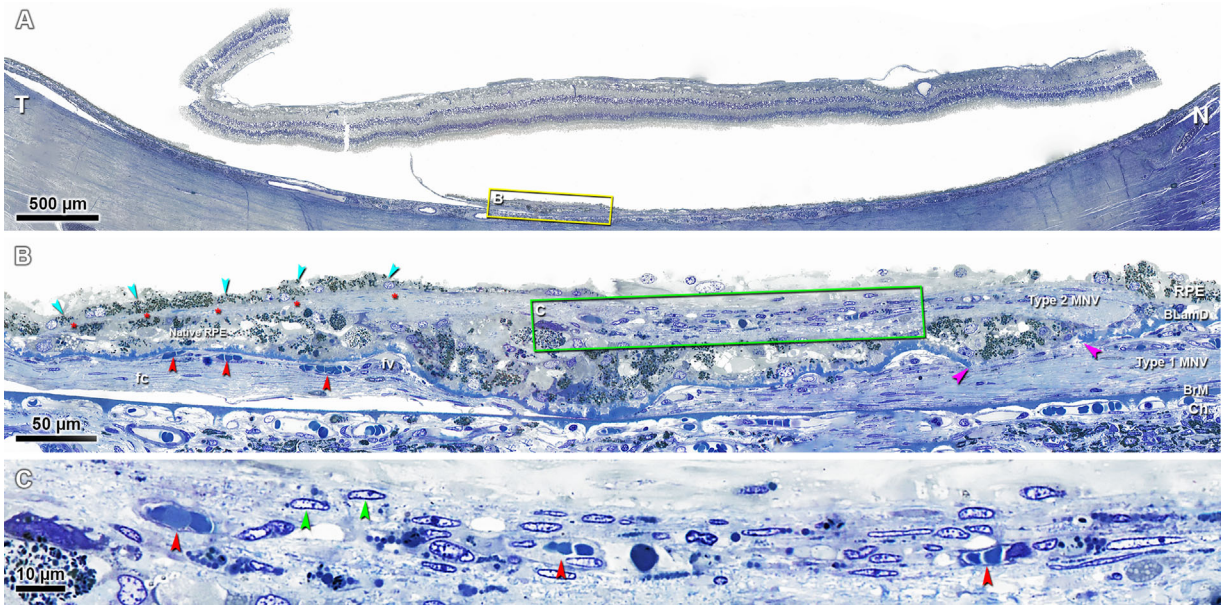

Figure 5. Mixed type 1 and 2 MNV: RPE enveloping the margin of type 2 MNV. Submicrometer epoxy resin sections of osmium-tannic acid-paraphenylenediamine post-fixed tissue were stained with toluidine blue. (A) Panoramic view of a section that passes through the inferior macula. Retina was post-mortem completely detached from RPE in this section but was attached near the optic nerve head in other sections. Yellow frame shows a region magnified in (B). (B) Type 2 MNV was on the top of BLamD and native RPE, which covered the type 1 MNV. On the left third of area with type 2 MNV tissue (red asterisks), the RPE (teal arrowheads) lacking BLamD enveloped the type 2 MNV. BLamD was continuous except at the right side, where a BLamD defect can be observed (between pink arrowheads). Type 1 MNV was underneath the RPE-BL. Fibrovascular (fv) and fibrocellular (fc) membranes were shown inside type 1 MNV tissue. Three vessel lumens align along the RPE-BL (red arrowheads; neochoriocapillaris[9]). Green frame shows an area magnified in (C). (C) Three vessel lumens (red arrowheads), not adjacent to the RPE and thus unlike type 1 MNV, were revealed inside Type 2 MNV. Many pericytes (green arrowheads) could be observed as well. BLamD, basal laminar deposit; Ch, choroid; N, nasal; T, temporal.

ChC densities were 0.42 ± 0.09, 0.37 ± 0.16, and 0.05 ± 0.02, in native ChC underneath MNV, ChC inside type 1 MNV, and ChC underneath atrophy, respectively.

Figure 6 shows type 1 and 2 MNV and atrophy on a section through the inferior macula. Retinal tissue, presumed to be largely Müller glia because it resembled photoreceptor-depleted ONL–HFL in the neurosensory retina, covered the type 2 MNV (Figs. 6A, 6B), BrM in atrophic area (Figs. 6A, 6C), and persistent BLamD on top of type 1 MNV (Figs. 6A, 6D). In another section, retina tissue traversed a defect in the RPE–BLamD complex and entered the type 1 MNV tissue (Fig. 6E). This same tissue traversed the BrM defect in an outward direction and invaded the choroid (Figs. 6F, 6G). Definitive marker studies to determine Müller cell identity were not possible with our tissue preparation technique.

The RPE layer in this case was continuous, except in the atrophic area, where it was completely absent. Figure 7 shows how the continuous layer transdifferentiated from RPE cells with normal spindle-shaped melanosomes to transitional cells with two melanosome types, then to melanotic cells with only spherical melanosomes, in a section near the atrophic area in inferior macula (Fig. 7A). Magnified images show age-normal nonuniform RPE with continuous BLamD above the type 1 MNV (Fig. 7B), depigmented RPE with darkly stained cytoplasm and multiple nuclei (Fig. 7C), RPE with spherical black organelles above and inside the type 1 MNV (Fig. 7D), RPE-derived cells[30] crossing the BrM defect (Fig. 7E), and RPE-derived cells and melanocytes in the choroid (Fig. 7F). Further magnification shows RPE with mainly spindle-shaped organelles (Fig. 7G), RPE with three nuclei and few organelles (Fig. 7H), RPE with spherical black organelles and two nuclei (Fig. 7I), RPE-derived cells with polydisperse spherical and spindle-shaped organelles as well as three nuclei (Fig. 7J), and RPE-derived cells with spherical organelles only and three nuclei (Fig. 7K). All RPE and RPE-derived cells are clearly distinguishable from choroidal melanocytes, which have very small, spherical, and densely packed greenish melanosomes (Fig. 7K).

By histology (Fig. 8), an area lacking photoreceptors inferior and temporal to the fovea corresponded with the cRORA spot seen clinically (Figs. 1–3). ELM descents, considered the border

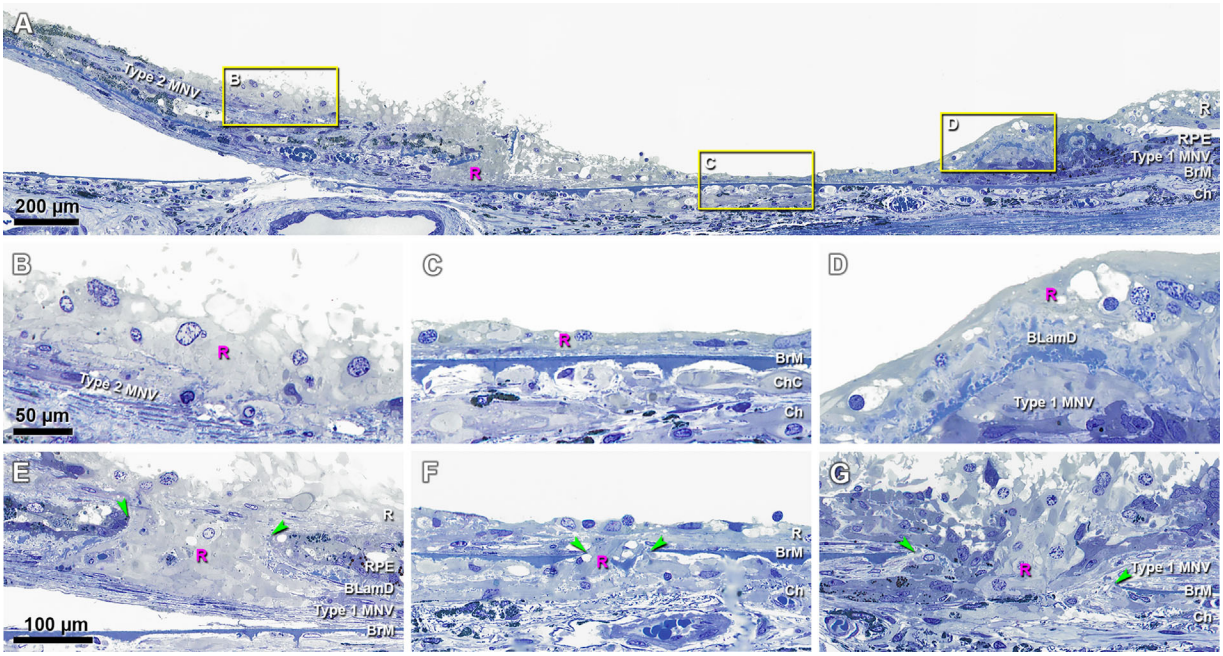

Figure 6. Retinal tissue contacts type 2 MNV and enters type 1 MNV and choroid. Submicrometer epoxy resin sections of osmium–tannic acid–paraphenylenediamine post-fixed tissue were stained with toluidine blue. (A) A section passing through the inferior macula shows type 2 MNV on the left third, atrophic area on the middle third and type 1 MNV on left and right thirds of this panel. Retinal tissue (presumably Müller glia) covered the type 2 MNV (frame B), BrM (frame C), and persistent BLamD (frame D). Yellow frames are magnified in B–D. (B) Retinal tissue covered the type 2 MNV. (C) Retinal tissue was found internal to BrM. (D) Retinal tissue covered persistent BLamD above the type 1 MNV. (E) Retinal tissue traversed a defect in RPE-BLamD (green arrowheads) and entered the type 1 MNV area (in a different section from A). (F–G) Retinal tissue traversed the BrM defect (green arrowheads) and entered the choroid (in a different section from A). BrM on the right side in G was depressed into the choroid. Scale bar in B applies to B–D; Scale bar in E applies to E–G. R, retinal tissue; BLamD, basal laminar deposit; Ch, choroid.

of atrophy in the photoreceptor layer,[8] were found in neurosensory retina and in retinal fragments adhered to RPE choroid (Tables 2 and 3). A section through the inferior macula shows LHEP on the inner retinal surface (Fig. 8A) and the atrophic area in outer retina bounded by two ELM descents (Fig. 8C). Immediately adjacent to the atrophic area, the ONL is thinned, outer segments are absent and inner segments are short. At 400 µm from the ELM descent the HFL/ONL is dyslaminate,[8] that is, lacking distinct layers owing to inward translocation of photoreceptor cell bodies (Fig. 8D). At a further distance is an extensive region with ordered HFL, thick ONL and healthy-appearing photoreceptors (Fig. 8B). In the fovea (not shown), cones were present, in greatly reduced numbers.

Discussion

We report a clinicopathologic correlation of a mixed type 1 and type 2 MNV secondary to AMD, underneath and adjacent to an area with drusen-associated atrophy, in an eye with multimodal imaging and anti-VEGF treatment over a long follow-up period. Our results show that a SIRE on OCT correlates on histology to type 1 MNV with neochoriocapillaris that is present at similar density to native ChC despite 3 years of continuous anti-VEGF therapy. An envelopment of type 2 MNV by RPE was seen in in vivo clinical imaging and in histology. Atrophy at one location corresponded with a clinically observed druse and was spatially and temporally dissociated from the onset of MNV. The initiation and enlargement of drusen-associated cRORA contrasted with the persistence of RPE and some photoreceptors over the MNV during follow-up. The choroidal invasion by presumably gliotic Müller cells in this case was notable. Specific RPE phenotypes were involved in the atrophic and neovascular processes.

In AMD type 1, MNV initiates from the choroid, and type 2 from it, and they ramify in different spaces (sub–RPE-BL and subretinal, respectively). Currently, the anatomic location of MNV can be determined by OCT imaging, and type 1 and type 2 MNV are considered OCT-based terms.[4,31] Defining these compartments can be challenging if continuous RPE layer is absent, and thus BLamD persisting after

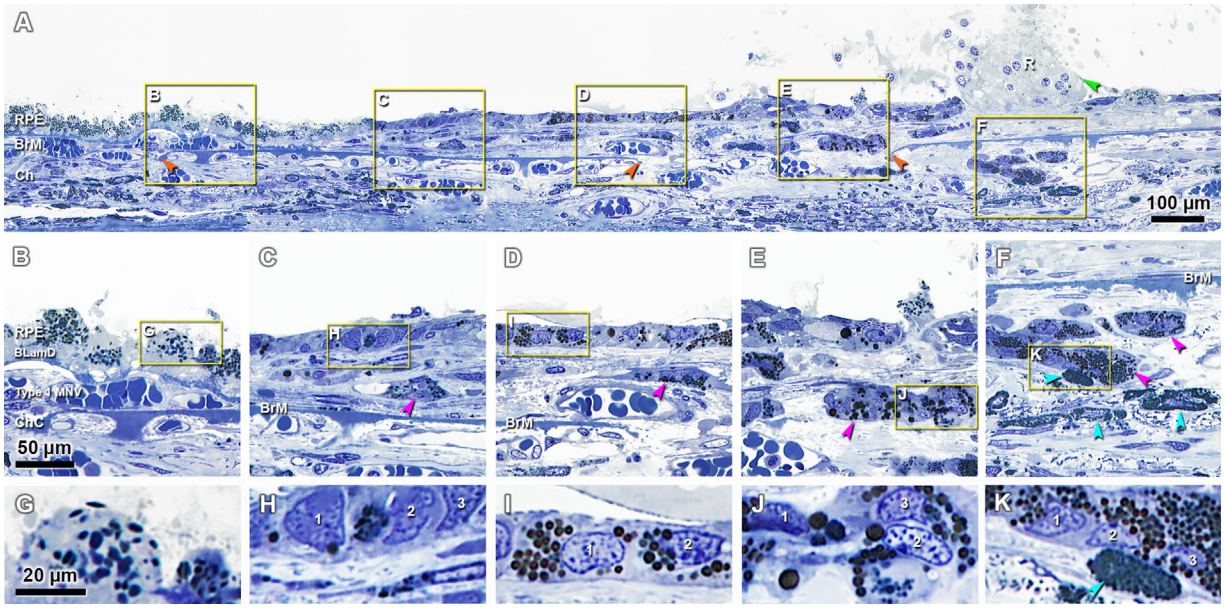

Figure 7. RPE cells become "melanotic" and enter the type 1 MNV and choroid. Submicrometer epoxy resin sections of osmium–tannic acid–paraphenylenediamine post-fixed tissue were stained with toluidine blue. (A) Panoramic view of a section passing close to the atrophic area in the inferior macula, shows how RPE cells transition from normal to melanotic. Orange arrowheads, BrM defect; Green arrowhead, descent of the ELM. Yellow frames in A are magnified in B–F. (B) Nonuniform RPE and continuous BLamD above the type 1 MNV. (C) Depigmented RPE have darkly stained cytoplasm and multiple nuclei. BLamD disappeared in this area with an RPE-derived cell inside the type 1 MNV (pink arrowhead). (D) RPE with dark spherical organelles overlaid the type 1 MNV. BLamD disappeared in this area. An RPE-derived cell with dark spherical organelles was inside the type 1 MNV (pink arrowhead). (E) In the BrM defect area, an RPE-derived cell (pink arrowhead) was crossing the defect. (F) Several RPE-derived cells (pink arrowheads) and melanocytes (teal arrowheads) were found in the choroid. Yellow frames highlighting cells in B–F are magnified in G–K, respectively. (G) RPE with mainly spindle shaped organelles. (H) RPE with three nuclei and few organelles. (I) RPE with dark spherical organelles and two nuclei. (J) RPE-derived cell with polydisperse spherical and spindle shaped organelles as well as three nuclei, from a neighboring serial section. (K) RPE-derived cell with darkly spherical organelles and three nuclei was distinct from a melanocyte (teal arrowhead) with denser and smaller organelles. Scale bar in B applies to B-F; Scale bar in G applies to G–K. BLamD, basal laminar deposit; Ch, choroid.

RPE disappearance is a landmark defining the original sub–RPE-BL space.[21,32] In the index case, definitive type 1 MNV, that is, bounded anteriorly by RPE with BLamD, was continuous with MNV bounded anteriorly by only thick persistent BLamD (Fig. 6D), also considered type 1. Types 1 and 2 MNV in this case both featured fibrovascular scar but differed in the location of vessels relative to RPE (near RPE for type 1, Fig. 5B)[9] and separated from it, for type 2). Type 1 and type 2 MNV are both choroid-originated and often occur together.[4] In a series of 266 newly presenting cases of MNV in AMD,[33] 39.9% were type 1, 9.0% were type 2, and 16.9% were mixed; of the mixed cases, 80.0% were types 1 and 2. However, type 2 can also occur suddenly in AMD eyes with subretinal drusenoid deposits and lacking soft drusen [34] and also in myopia and other maculopathies.

The regression of type 2 MNV into a type 1 pattern with envelopment by the RPE has been clinically described in anti-VEGF–treated neovascular AMD.[35] This phenomenon was also observed in eyes with pathologic myopia, multifocal choroiditis, and other inflammatory conditions.[36,37] In the index case, type 2 MNV was enveloped at the margins by RPE, shown in both clinical images and histology sections. Our results highlight a role of RPE envelopment in limiting type 2 MNV lesions and potentially protecting neuroretina from harm. The middle part of type 2 MNV was contacted by retina tissue (presumably Müller glia, Fig. 6) that also covered BrM in the atrophic area[38] and in the type 1 MNV area, persistent BLamD. The possibility that Müller glia are also protective cannot be readily assessed in this specimen because of the noncorrespondence of detached retina and RPE–choroid layers.

The transition from drusen to atrophy also involves neurosensory retina, as recently defined in studies linking clinical imaging to comprehensive histology like that used herein.[8,13–15,28] These studies showed RPE dying or migrating off the top of drusen into the retina, degeneration and loss of photoreceptors, drusen acquiring calcific nodules as tombstone lesions, and invasion of Müller glia through persistent BLamD into the sub–RPE-BL space. The index case seemed

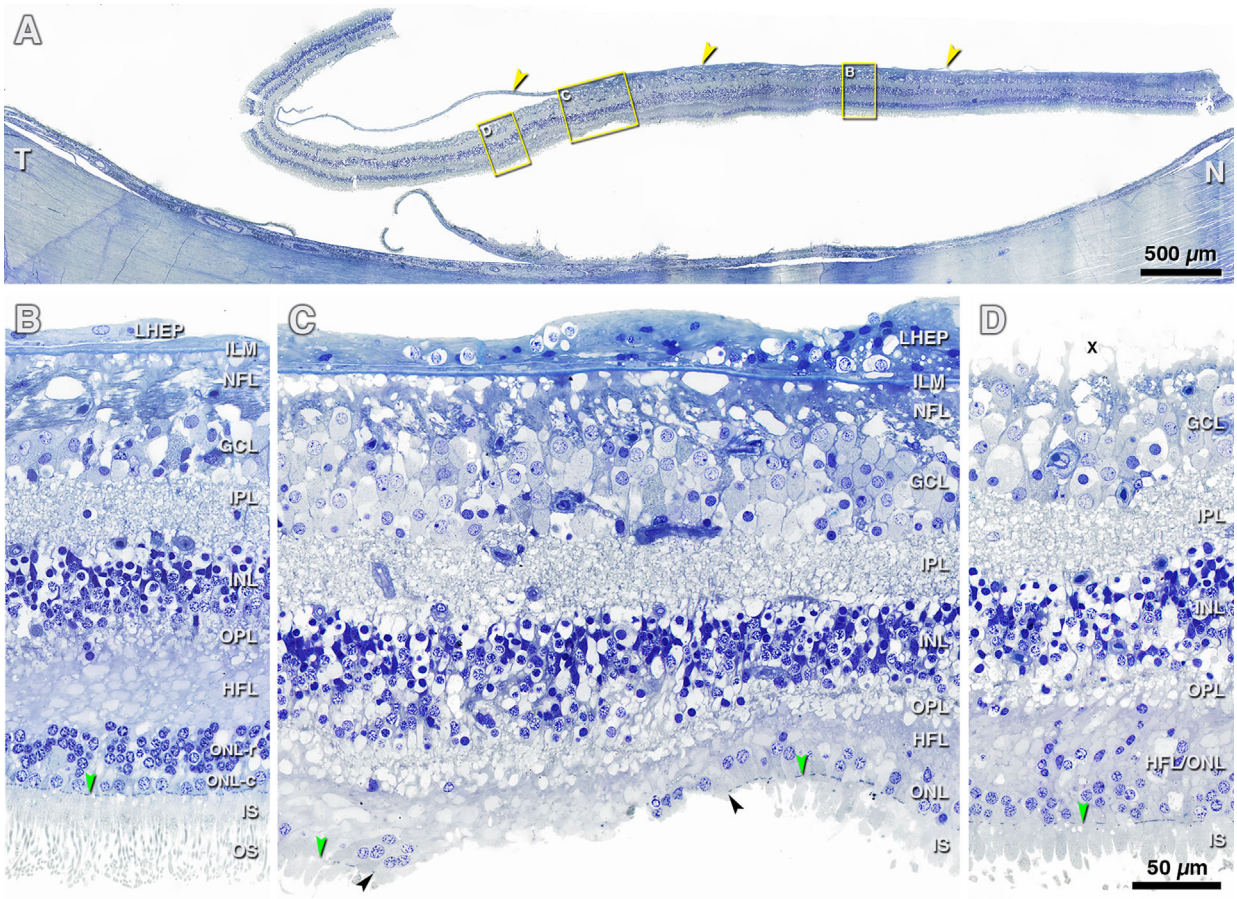

Figure 8. Histology of drusen-associated atrophy of retina. Submicrometer epoxy resin sections of osmium–tannic acid–paraphenylenediamine post-fixed tissue were stained with toluidine blue. (A) Panoramic view of a section passing through the inferior macula. Retina was completely detached from RPE in this section. Lamellar hole-associated epiretinal proliferation (LHEP, yellow arrowheads) covered the inner surface of retina and was partly detached on the temporal side. Yellow frames are magnified in B–D. (B) 1470 µm away from the border of drusen-associated atrophy. Normal retina with an ordered HFL, thick ONL with multiple rod layers and single cone layer, and healthy-appearing photoreceptors. (C) Atrophic area (between black arrowheads) is bounded by a descent of ELM (green arrowheads) on both sides. Around the atrophic area, the ONL is thinner, with only one or two layers of nuclei. OS are absent and IS are short in this area. The INL overlying the atrophic area is disorganized. (D) Image is 400 µm away from the border of drusen-associated atrophy. The distinction between HFL and ONL is lost owing to dyslamination. OS are absent and IS are short. GCL, ganglion cell layer; ILM, internal limiting membrane; INL, inner nuclear layer; IPL, inner plexiform layer; IS, inner segment; N, nasal; NFL, nerve fiber layer; ONL-r, rods; ONL-c, cones; OPL, outer plexiform layer; OS, outer segment; T, temporal. X, artifact owing to detachment of LHEP. Scale bar in D applies to B–D.

to exhibit this same sequence of drusen-associated atrophy over a 3.8-year follow-up: drusen with overlying HRF at baseline, enlargement and inward migration of intraretinal HRF, drusen collapse, and loss of photoreceptors. After this collapse, type 1 MNV arose in a nearby location, where RPE was apparently intact enough to secrete VEGF.

Progression to atrophy, including an ELM descent toward BrM, an indicator of Müller cell gliosis and adhesion, was observed in the index case. Recently, gliotic Müller cell processes were demonstrated in the subretinal space in areas of RPE atrophy and also over individual drusen that were denuded of RPE.[38] We observed in histology that the ELM dropped onto individual drusen, putting Müller glia in direct contact with remaining BLamD.[15] A novel finding in this study is that Müller glia traversed RPE-BL and BrM and entered both type 1 MNV and choroid (Figs. 6E–6G). Glial seal, that is, penetration of reactive Müller glia into the sub–RPE-BL space, was previously observed by histology.[38–41] Müller glia entering choroid has not been reported in AMD, but OCT signatures suggesting retinal intrusion past BrM can appear in other diseases.[42] Why this occurs is currently unclear, yet we can speculate that the combination of Müller cell entry into drusen plus an opportune break in BrM may have been contributory in this case. We also cannot exclude an impact of the LMH on adjacent Müller glia.

RPE plays vital roles in visual function and preserving the integrity of neighboring cells; in AMD, RPE

has multiple fates. These include but are not limited to death in place, anterior migration into the retina, and transdifferentiation.[16,43] RPE activation and migration into the retina, manifest as intraretinal HRF in OCT and observed in the index case (Fig. 3), is a high-risk precursor to advanced AMD.[44,45] Anterior migration is plausibly driven by hypoxia, based on the previous observation of RPE cells correlating with HRF-adjoining retinal capillaries.[10,46] The continuity of RPE over type 1 MNV, plus the persistence of some photoreceptors over MNV during follow-up, supports the concept that the outer retinal structure can benefit from type 1 MNV[9] in some patients. In the index case, cRORA initiated at a druse was in close proximity to MNV. In this location, the cRORA expanded more slowly than in eyes with non-neovascular AMD, using the effective radius growth rate as a metric.[26] Prior clinical studies showed that type 1 MNV decreased the risk for atrophy progression.[47–49] In this case, however, we could not assess the impact of type 1 MNV in isolation, owing to the presence of type 2 MNV.

Although the RPE was continuous over the type 1 MNV, it is not completely normal, because we observed a morphologic transdifferentiation of these cells (Fig. 7) distinct from the progressive RPE dysmorphia seen in geographic atrophy. In published surveys of anonymous donor eyes, transdifferentiation between phenotypes was supported by the demonstration of transitional morphologies in single continuous histologic sections.[30] In this clinically documented eye, we clearly show the continuity of RPE cells converting from age-normal into melanotic cells with large spherical melanosomes (Fig. 7), and we directly compare them with native choroidal melanocytes with small spherical melanosomes (Figs. 7F, 7K). Melanotic cells did not seem to have arisen from RPE cells entombed within fibrovascular scars, as suggested.[30] Also in this case, melanotic cells had multiple nuclei and invaded the type 1 MNV and choroid, for reasons that remain to be determined, but may include the presence of extended and enabling Müller glia. Melanotic cells likely account for the black pigment frequently seen in eyes with neovascular AMD, but we cannot herein assess that possibility, owing to the long interval between color fundus photography and death.

The strengths of this study are the OCT-anchored multimodal clinical imaging with long follow-up, a short interval of 2 months between the last clinic visit and death, high-resolution comprehensive histology in an intact eye, a growing knowledge base from our prior studies of neovascular AMD, and multiscale photodocumentation. Limitations are pathology complicated by the presence of LHEP and LMH as well as postmortem retinal detachment and lateral torsion. Nevertheless, LHEP and LMH in this eye was stable for a long period,[22] and many features were observed on both histology sections and OCT B-scans.

We present the first clinicopathologic correlation of drusen-associated atrophy with a mixed type 1 and 2 MNV, in an eye that received continuous anti-VEGF for approximately 3 years with nearly stable best-corrected visual acuity of 20/50. By differentiating progression sequences associated with drusen and with MNV, we suggest that type 1 MNV can sustain RPE and decrease the extent of overlying photoreceptor atrophy. In contrast, photoreceptor loss after RPE disappearance and drusen collapse is absolute. Further, type 2 MNV can regress into a type 1 pattern by RPE envelopment of neovascular tissue. Therefore, two treatment strategies supported by our results are maintaining type 1 MNV to preserve RPE and targeting drusen to prevent severe atrophy. Focused investigation of these ideas in patients where glial involvement in MNV is not complicated by LMH will be informative.

Acknowledgments

We thank The Eye-Bank for Sight Restoration (NYC) for timely retrieval of donor eyes and K.R. Sloan PhD with ImageJ analysis.

Supported by Genentech/Hoffman LaRoche, Heidelberg Engineering, The Macula Foundation, Inc., New York, NY; unrestricted funds to the Department of Ophthalmology and Visual Sciences (UAB) from Research to Prevent Blindness, Inc., and EyeSight Foundation of Alabama.

Disclosure: **L. Chen,** None; **M. Li,** None; **J.D. Messinger,** None; **D. Ferrara,** Genentech (E); **C.A. Curcio,** Genentech (C), Hoffman LaRoche (C), Novartis (C), Heidelberg Engineering (C); **K.B. Freund,** Genentech (C), Optovue (C), Zeiss (C), Heidelberg Engineering (C), Allergan (C), Novartis (C)

Note added in proof: While this paper was in review, Hubschman et al published a consensus definition for lamellar macular hole based on OCT imaging and recommended that "lamellar-macular hole associated epiretinal proliferation", as seen in our case, be called simply "epiretinal proliferation" because it is not specific to lamellar hole.

Hubschman, J. P., Govetto, A., Spaide, R. F., Schumann, R., Steel, D., Figueroa, M. S., Sebag, J., Gaudric, A., Staurenghi, G., Haritoglou, C.,

Kadonosono, K., Thompson, J. T., Chang, S., Bottoni, F., Tadayoni, R., 2020. Optical coherence tomography-based consensus definition for lamellar macular hole. *Br J Ophthalmol*. PMID 32107208.

References

1. Flaxman SR, Bourne RRA, Resnikoff S, et al. Global causes of blindness and distance vision impairment 1990-2020: a systematic review and meta-analysis. *Lancet Glob Health*. 2017;5:e1221–e1234.
2. Maguire MG, Martin DF, Ying GS, et al. Five-year outcomes with anti-vascular endothelial growth factor treatment of neovascular age-related macular degeneration: the comparison of age-related macular degeneration treatments trials. *Ophthalmology*. 2016;123:1751–1761.
3. Bhisitkul RB, Mendes TS, Rofagha S, et al. Macular atrophy progression and 7-year vision outcomes in subjects from the ANCHOR, MARINA, and HORIZON studies: the SEVEN-UP study. *Am J Ophthalmol*. 2015;159:915–924.e2.
4. Spaide RF, Jaffe GJ, Sarraf D, et al. Consensus nomenclature for reporting neovascular age-related macular degeneration data: consensus on neovascular age-related macular degeneration nomenclature study group. *Ophthalmology*. 2019;127:616–636.
5. Sarks JP, Sarks SH, Killingsworth MC. Morphology of early choroidal neovascularisation in age-related macular degeneration: correlation with activity. *Eye (Lond)*. 1997;11:515–522.
6. Spaide RF, Armstrong D, Browne R. Continuing medical education review: choroidal neovascularization in age-related macular degeneration–what is the cause? *Retina*. 2003;23:595–614.
7. Curcio CA, Balaratnasingam C, Messinger JD, Yannuzzi LA, Freund KB. Correlation of type 1 neovascularization associated with acquired vitelliform lesion in the setting of age-related macular degeneration. *Am J Ophthalmol*. 2015;160:1024–1033.e3.
8. Li M, Huisingh C, Messinger J, et al. Histology of geographic atrophy secondary to age-related macular degeneration: a multilayer approach. *Retina*. 2018;38:1937–1953.
9. Chen L, Messinger JD, Sloan KR, et al. Nonexudative macular neovascularization supporting outer retina in age-related macular degeneration: a clinicopathologic correlation. *Ophthalmology*. 2020;127:931–947.
10. Li M, Dolz-Marco R, Messinger JD, et al. Clinicopathologic correlation of anti-vascular endothelial growth factor-treated type 3 neovascularization in age-related macular degeneration. *Ophthalmology*. 2018;125:276–287.
11. Sadda SR, Guymer R, Holz FG, et al. Consensus definition for atrophy associated with age-related macular degeneration on OCT: classification of atrophy report 3. *Ophthalmology*. 2018;125:537–548.
12. Sarks JP, Sarks SH, Killingsworth MC. Evolution of geographic atrophy of the retinal pigment epithelium. *Eye (Lond)*. 1988;2:552–577.
13. Li M, Dolz-Marco R, Huisingh C, et al. Clinicopathologic correlation of geographic atrophy secondary to age-related macular degeneration. *Retina*. 2019;39:802–816.
14. Tan ACS, Pilgrim MG, Fearn S, et al. Calcified nodules in retinal drusen are associated with disease progression in age-related macular degeneration. *Sci Transl Med*. 2018;10:eaat4544.
15. Guymer RH, Rosenfeld PJ, Curcio CA, et al. Incomplete retinal pigment epithelial and outer retinal atrophy in age-related macular degeneration: classification of atrophy meeting report 4. *Ophthalmology*. 2020;127:394–409.
16. Curcio CA, Zanzottera EC, Ach T, Balaratnasingam C, Freund KB. Activated retinal pigment epithelium, an optical coherence tomography biomarker for progression in age-related macular degeneration. *Invest Ophthalmol Vis Sci*. 2017;58:BIO211–BIO26.
17. Ach T, Tolstik E, Messinger JD, Zarubina AV, Heintzmann R, Curcio CA. Lipofuscin redistribution and loss accompanied by cytoskeletal stress in retinal pigment epithelium of eyes with age-related macular degeneration. *Invest Ophthalmol Vis Sci*. 2015;56:3242–3252.
18. Gambril JA, Sloan KR, Swain TA, et al. Quantifying retinal pigment epithelium dysmorphia and loss of histologic autofluorescence in age-related macular degeneration. *Invest Ophthalmol Vis Sci*. 2019;60:2481–2493.
19. Sarks J, Tang K, Killingsworth M, Arnold J, Sarks S. Development of atrophy of the retinal pigment epithelium around disciform scars. *Br J Ophthalmol*. 2006;90:442–446.
20. Litts KM, Messinger JD, Freund KB, Zhang Y, Curcio CA. Inner segment remodeling and mitochondrial translocation in cone photoreceptors in age-related macular degeneration with outer retinal tubulation. *Invest Ophthalmol Vis Sci*. 2015;56:2243–2253.

21. Zanzottera EC, Ach T, Huisingh C, Messinger JD, Spaide RF, Curcio CA. Visualizing retinal pigment epithelium phenotypes in the transition to geographic atrophy in age-related macular degeneration. *Retina*. 2016;36(Suppl 1):S12–S25.
22. Pang CE, Spaide RF, Freund KB. Epiretinal proliferation seen in association with lamellar macular holes: a distinct clinical entity. *Retina*. 2014;34:1513–1523.
23. Xu X, Liu X, Wang X, et al. Retinal pigment epithelium degeneration associated with subretinal drusenoid deposits in age-related macular degeneration. *Am J Ophthalmol*. 2017;175:87–98.
24. Curcio CA, Millican CL, Bailey T, Kruth HS. Accumulation of cholesterol with age in human Bruch's membrane. *Invest Ophthalmol Vis Sci*. 2001;42:265–274.
25. Pang CE, Messinger JD, Zanzottera EC, Freund KB, Curcio CA. The onion sign in neovascular age-related macular degeneration represents cholesterol crystals. *Ophthalmology*. 2015;122:2316–2326.
26. Shen L, Liu F, Grossetta Nardini H, Del Priore LV. Natural history of geographic atrophy in untreated eyes with nonexudative age-related macular degeneration: a systematic review and meta-analysis. *Ophthalmol Retina*. 2018;2:914–921.
27. Mones J, Biarnes M, Trindade F. Hyporeflective wedge-shaped band in geographic atrophy secondary to age-related macular degeneration: an underreported finding. *Ophthalmology*. 2012;119:1412–1419.
28. Tan ACS, Astroz P, Dansingani KK, et al. The evolution of the plateau, an optical coherence tomography signature seen in geographic atrophy. *Invest Ophthalmol Vis Sci*. 2017;58:2349–2358.
29. Dolz-Marco R, Glover JP, Gal-Or O, et al. Choroidal and sub-retinal pigment epithelium caverns: multimodal imaging and correspondence with Friedman lipid globules. *Ophthalmology*. 2018;125:1287–1301.
30. Zanzottera EC, Messinger JD, Ach T, Smith RT, Curcio CA. Subducted and melanotic cells in advanced age-related macular degeneration are derived from retinal pigment epithelium. *Invest Ophthalmol Vis Sci*. 2015;56:3269–3278.
31. Freund KB, Zweifel SA, Engelbert M. Do we need a new classification for choroidal neovascularization in age-related macular degeneration? *Retina*. 2010;30:1333–1349.
32. Green WR, Enger C. Age-related macular degeneration histopathologic studies. the 1992 Lorenz E. Zimmerman lecture. *Ophthalmology*. 1993;100:1519–1535.
33. Jung JJ, Chen CY, Mrejen S, et al. The incidence of neovascular subtypes in newly diagnosed neovascular age-related macular degeneration. *Am J Ophthalmol*. 2014;158:769–779.e2.
34. Naysan J, Jung JJ, Dansingani KK, Balaratnasingam C, Freund KB. Type 2 (subretinal) neovascularization in age-related macular degeneration associated with pure reticular pseudodrusen phenotype. *Retina*. 2016;36:449–457.
35. Dolz-Marco R, Phasukkijwatana N, Sarraf D, Freund KB. Regression of type 2 neovascularization into a type 1 pattern after intravitreal antivascular endothelial growth factor therapy for neovascular age-related macular degeneration. *Retina*. 2016;37:222–233.
36. Battaglia Parodi M, Iacono P, Bandello F. Correspondence of leakage on fluorescein angiography and optical coherence tomography parameters in diagnosis and monitoring of myopic choroidal neovascularization treated with bevacizumab. *Retina*. 2016;36:104–109.
37. Vance SK, Khan S, Klancnik JM, Freund KB. Characteristic spectral-domain optical coherence tomography findings of multifocal choroiditis. *Retina*. 2011;31:717–723.
38. Edwards MM, McLeod DS, Bhutto IA, Grebe R, Duffy M, Lutty GA. Subretinal glial membranes in eyes with geographic atrophy. *Invest Ophthalmol Vis Sci*. 2017;58:1352–1367.
39. Curcio CA, Medeiros NE, Millican CL. Photoreceptor loss in age-related macular degeneration. *Invest Ophthalmol Vis Sci*. 1996;37:1236–1249.
40. Anderson DH, Guerin CJ, Erickson PA, Stern WH, Fisher SK. Morphological recovery in the reattached retina. *Invest Ophthalmol Vis Sci*. 1986;27:168–183.
41. Chen L, Messinger JD, Zhang Y, Spaide RF, Freund KB, Curcio CA. Subretinal drusenoid deposit in age-related macular degeneration: histologic insights into initiation, progression to atrophy, and imaging. *Retina*. 2019;40:618–631.
42. Zhang X, Zuo C, Li M, Chen H, Huang S, Wen F. Spectral-domain optical coherence tomographic findings at each stage of punctate inner choroidopathy. *Ophthalmology*. 2013;120:2678–2683.
43. Fuhrmann S, Zou C, Levine EM. Retinal pigment epithelium development, plasticity, and tissue homeostasis. *Exp Eye Res*. 2014;123:141–50.
44. Ferrara D, Silver RE, Louzada RN, Novais EA, Collins GK, Seddon JM. Optical coherence tomography features preceding the onset of advanced age-related macular degeneration. *Invest Ophthalmol Vis Sci*. 2017;58:3519–3529.

45. Nassisi M, Lei J, Abdelfattah NS, et al. OCT risk factors for development of late age-related macular degeneration in the fellow eyes of patients enrolled in the HARBOR study. *Ophthalmology*. 2019;126:1667–1674.
46. Balaratnasingam C, Messinger JD, Sloan KR, Yannuzzi LA, Freund KB, Curcio CA. Histologic and optical coherence tomographic correlates in drusenoid pigment epithelium detachment in age-related macular degeneration. *Ophthalmology*. 2017;124:644–656.
47. Xu L, Mrejen S, Jung JJ, et al. Geographic atrophy in patients receiving anti-vascular endothelial growth factor for neovascular age-related macular degeneration. *Retina*. 2015;35:176–186.
48. Christenbury JG, Phasukkijwatana N, Gilani F, Freund KB, Sadda S, Sarraf D. Progression of macular atrophy in eyes with type 1 neovascularization and age-related macular degeneration receiving long-term intravitreal antivascular endothelial growth factor therapy: an optical coherence tomographic angiography analysis. *Retina*. 2018;38:1276–1288.
49. Dhrami-Gavazi E, Balaratnasingam C, Lee W, Freund KB. Type 1 neovascularization may confer resistance to geographic atrophy amongst eyes treated for neovascular age-related macular degeneration. *Int J Retina Vitreous*. 2015;1:15.